Real-time critical marine infrastructure multi-sensor surveillance via a constrained stochastic coverage algorithm

F Ponzini[a], C Fruzzetti[a,*], N Sabatino[a]

[a]*Department of Marine, Electrical, Electronic, Telecomunications Engineering and Naval Architecture (DITEN), Polytechnic School of Genoa University*

*Email: camilla.fruzzetti@edu.unige.it

Synopsis

In recent years, monitoring and protecting marine infrastructure have become increasingly critical. Surface marine vessels can provide valuable support in monitoring structures such as offshore wind farms, data cables, and pipelines. Employing surface vessels with ever-increasing autonomous capabilities allows for increased operation efficiency and strategic advantages. In critical infrastructure monitoring, the area of interest is known in advance, and the aim is to detect anomalies. This paper focuses on developing a guidance, navigation, and control framework suitable for a MASS and tailored for critical infrastructure monitoring missions. The primary goals are developing a stochastic-based coverage algorithm to ensure the surveillance of an area of interest and a real-time compliant shadow vessels monitoring system that provides situational awareness of the above-water surrounding environment, detecting threats and unexpected targets over time. The navigation in the operational environment is ensured by an appropriate proprioceptive sensing layer. The hypotheses and the methodologies are shown and explained in detail, together with the preliminary results reporting the first integration. The results are obtained via computer simulations applied to a wind farm critical infrastructure scenario; additional experimental tests are carried out in indoor and outdoor controlled environments to assess the proposed navigation and control systems capability, involving a marine autonomous surface ships test platform available in the university laboratory. The preliminary results demonstrate the ability of the systems to cooperate in the proposed architecture, monitor an Area Of Interest, detect threats, effectively manoeuvre the vessel in real-time, and estimate its state. Such a framework can be further enhanced by extending the perception capabilities for the underwater domain, integrating multiple control logic to allow for more efficient surveillance strategies, or extending the vessel capabilities beyond surveillance missions, adding capabilities like target chasing.

Keywords: GNC, MASS, critical infrastructure surveillance, dark ship detection, coverage algorithm, situational awareness

1 Introduction

Ocean-related economic activities have experienced exponential growth in the last decades in their outputs and relevance for the global economy. Since the 1960s, offshore oil and gas extraction activities have constantly increased their volume and revenue to the point that a relevant share of global fossil fuels come from the seabed (Jouffray et al., 2020; Jolly, 2016). From 1980 to 2022, the output of container ship trade has quadrupled (UNCTAD, 2022), making maritime trade activities account for 80% of the global trade volume and 70% (UNCTAD, 2017) of its value. Together with well-established seaborne economic activities like trading, ports, and oil and gas extraction, many emerging industrial sectors are participating in this economic boom. Among them, offshore wind farm building and data cable laying will be pivotal in the future economic exploitation of the ocean. The offshore wind farm sector is experiencing high investments as a consequence of the energy transition (Commission, 2023), while more than 95% of all the data that moves around the world goes through undersea data cables, totalling over 900,000 miles sit on the ocean floor (Chataut, 2024), which are bound to increase. This growth of both established and emerging ocean-related economic activities is increasing the reliance of industries and whole countries on maritime infrastructures up to the point that they can now be considered critical for ensuring proper energy and food security as land-based resources rapidly become more scarce (Jouffray et al., 2020).

Threats to critical marine infrastructures may come in various forms, from unintentional harms (Clare, 2021) to deliberate acts (Bueger, 2023; Knights, 2024), usually carried on by dark ships/shadow vessels (Kantchev, 2023), i.e. ships that cover their true intentions by implementing concealing techniques, such as turning off their Automatic Identification System (AIS) device, spoofing their AIS location or using a flag of convenience (Nguyen,

Authors' Biographies

Filippo Ponzini was born in Italy in 1996. He received his B.Sc. and M.Sc. in Naval Architecture and Marine Engineering from Genoa University (Italy) in 2019, 2021. Since November 2022, he is a PhD student in Marine Science and Technologies at the DITEN department of Genoa University. His research activity mainly concerns navigation systems for autonomous vessels and multi-sensor data fusion.

Camilla Fruzzetti was born in Italy in 1995. She received the BSc, the MSs, and the PhD in Naval Architecture and Marine Engineering from the University of Genoa in 2017, 2019, and 2024, respectively. Since November 2023, she is a research fellow at the University of Genoa. Her main research interests concern ship guidance and control logic for autonomous navigation.

Nicola Sabatino was born in Italy in 1999. He studied Naval Architecture and Marine Engineering at the University of Genoa (Italy), earning his B.Sc. and his M.Sc in 2021 and 2023 respectively. He currently is a PhD student at the University of Genoa. His main research interests revolve around the application of symbolic artificial intelligence methods to the problems of autonomous marine collision avoidance.

 https://doi.org/10.24868/11141

2023). Critical marine infrastructure vastly differs from land-based ones, mainly because of the challenges posed by conducting operations at sea, so their protection requires tailored solutions. One of the primary solutions to ensure adequate protection of critical marine infrastructure is surveillance and monitoring using Maritime Autonomous Surface Ships (MASS) and Unmanned Underwater Vehicles (UUV) (Bueger and Liebetrau, 2023). Several works have been done in this direction in recent years, mainly thanks to the recent progress in Artificial Intelligence (AI), computing and communication technologies. (Manzari, 2020) and (Ferri et al., 2017) present surveys on significant applications of autonomous vehicles for surveillance operations, the first focusing on both MASSs and UUVs, the second on cooperative networks of UUVs.

The key features that a MASS/UUV-based platform needs for surveillance operations are coverage-driven guidance, collision-free path planning capabilities, and obstacle and target detection. A survey on coverage path planning algorithms is presented by (Tan et al., 2021), which focuses on deterministic algorithms; (Duan and Bullo, 2021), instead, reviews stochastic coverage algorithms based on Markov Chains. (Zadeh et al., 2022) illustrates an optimal collision-free path planning algorithm for multi-surface vessel missions employing particle swarm optimisation, while (Song et al., 2019) adopts the well-known A* algorithm for the same issue. (Zaccone, 2024) presents the use of Dynamic Programming algorithm for collision-free path planning of autonomous ships. The work in (Molina-Molina et al., 2021) describes the adoption of a MASS equipped with cameras for tackling the obstacle and target detection problem; the proposed system adopts deep learning techniques for target detection, which were tested in a port facility. (Zhang et al., 2021b) presents a study on using LiDAR (Light Detection and Ranging) and image processing to achieve target and obstacle detection with a MASS. (Birk et al., 2012) shows an example of a simulated surveillance operation using MASSs: as part of the European project "Cooperative Cognitive Control for Autonomous Underwater Vehicle", they carried out a simulation involving the use of a MASS swarm for a cooperative patrolling operation with a human scuba diver.

This paper presents an integrated solution for the live surveillance of critical marine infrastructure adopting a MASS. The proposed platform, driven by a constrained stochastic coverage algorithm based on Markov Chains, is designed to survey a known domain and detect the presence of shadow vessel intruders using onboard LiDAR. Recent applications (Karaki et al., 2022) have demonstrated the capabilities of such sensors in detecting obstacles and targets, even undetectable by RADARs (Radio Detection and Ranging), in both coastal (Faggioni et al., 2022a,b), and blue-water scenarios (Martelli et al., 2022). This cutting-edge application of MASSs showcases the potential of autonomous maritime technologies in enhancing the security of critical marine infrastructures. This paper presents the overall proposed framework, the single subsystems, and the preliminary results for the final system statement and integration. A testing campaign is carried out on a simulated scenario to evaluate the performances of the high-level guidance algorithms and the perceptive system. Moreover, a series of tests in a real controlled environment is performed to validate the control and state estimation system and interaction with the vessel.

2 Autonomous surveillance platform architecture

The autonomous surveillance platform proposed in this paper follows the Guidance, Navigation, and Control (GNC) paradigm, already widely employed in the literature for defining a MASS (Fossen, 2011). A functional scheme of the developed architecture is shown in Figure 1.

In this application, the guidance system aims to compute the desired pose $\boldsymbol{\eta}_D$ and the desired speed array $\boldsymbol{\nu}_D$ needed to satisfy the critical infrastructure monitoring goal. Its hierarchical structure can be split into three subsystems: the coverage algorithm, which acts as the high-level path planner and defines a target location $\mathbf{WP}_{target}$ to be reached starting from the coverage mission goal, data from Geographic Information System (GIS), and an occupancy grid computed by the navigation system; the collision-free path planning, which computes a path as a series of waypoints $\mathbf{WP}_{list}$ to reach $\mathbf{WP}_{target}$ and updates such path if risk of collision arises; the track keeping, which computes the desired pose $\boldsymbol{\eta}_{TR}$ and speed array $\boldsymbol{\nu}_{TR}$ at each time step needed to follow the defined path.

The control system receives as inputs the desired pose and speed array with their feedback values. To satisfy the guidance aim, it computes the appropriate forces and moment $\boldsymbol{\tau}_C$ in the ship reference frame. This architecture aims to control three Degrees Of Freedom (DOF) and is composed of: the controller, which computes the needed $\boldsymbol{\tau}_C$ to nullify the difference between the desired setpoints and the feedback values as done in (Donnarumma et al., 2022); the force allocation logic, necessary to coordinate the thrusts T_i and the relative angles α_i to be asked to each different actuators to produce $\boldsymbol{\tau}_C$ globally, it is solved with optimisation techniques as in (Fruzzetti et al., 2022); and the thrust allocation logic to compute the relative setpoints for each actuator (the pump-jet angles α_i and revolution speed n_i) thanks to combinator curves.

The desired setpoints are then sent to the MASS. The Shallow Water Autonomous Multipurpose Platform (SWAMP) full-electric catamaran (Odetti et al., 2020) is selected as a test case for the tests in the controlled environment since it is available in the university infrastructure. It can also be adopted for the future integration of the whole architecture and its relative test in a controlled environment representing a scaled model of a critical infrastructure. It is equipped with an Inertial Measurement Unit (IMU), Global Positioning System (GPS) receivers,

 https://doi.org/10.24868/11141

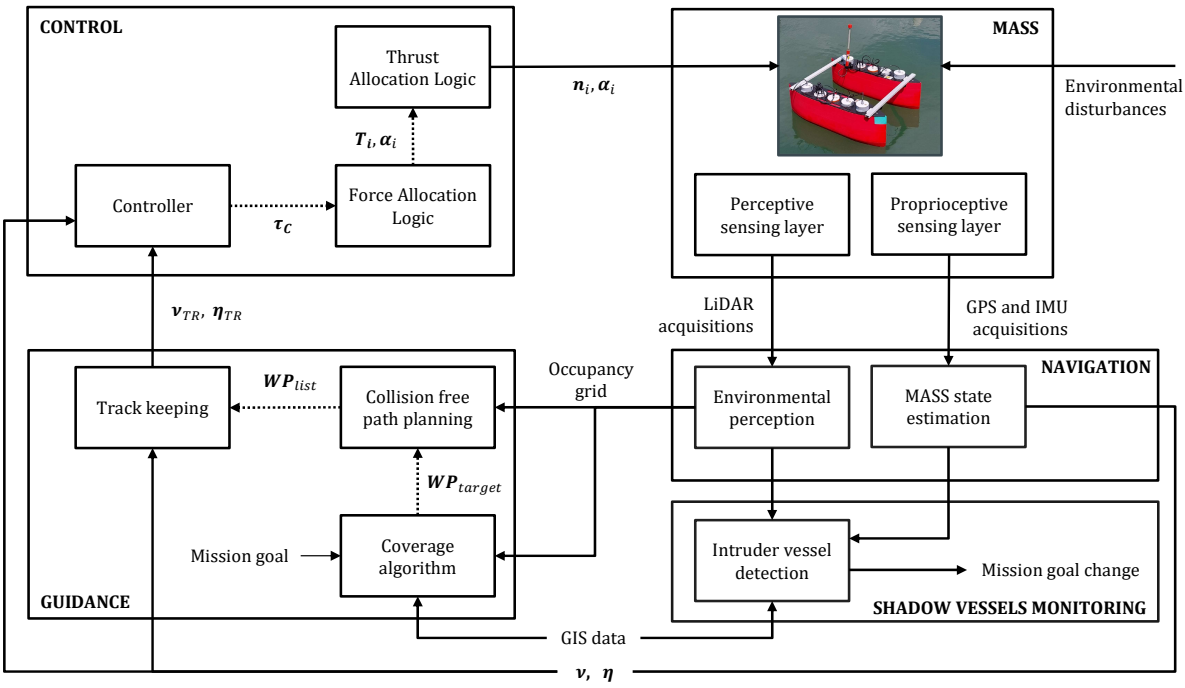

Figure 1: MASS architecture.

and a LiDAR, composing the proprioceptive and perceptive sensing layers of the Navigation system, while the communication is ensured by Wi-Fi.

The navigation system elaborates the information coming from the sensing layers. Two subsystems are present: the environmental perception and the MASS state estimation. The environmental perception module processes the acquisitions of the perceptive sensing layer and computes the obstacles occupancy grid of the operational domain; the MASS state estimation module processes the proprioceptive sensing layer outcome to estimate the vessel generalised pose ($\boldsymbol{\eta}$) and speed ($\boldsymbol{\nu}$).

The shadow vessels monitoring system is the core of the proposed architecture and monitors the operational domain. The inputs are the obstacle grid from the perceptive layer and the GIS data. The system continually analyses the acquisitions and compares them with the GIS data to detect shadow vessels. When the shadow vessel is detected, the surveillance mission can be concluded, and new logic can be triggered according to the operational scenario.

The communication middleware used among the previously described systems is implemented via the Message Queuing Telemetry Transport (MQTT) protocol (Yassein et al., 2017).

3 Reference frames and kinetics

This section presents the reference systems adopted within the paper and the transformations adopted between them. Figure 2 defines the reference frames that will be used throughout the paper:

- The n-frame $\{\boldsymbol{\Omega}, \underline{n}_i\}$ is an inertial Earth-fixed frame. The origin $\boldsymbol{\Omega}$ is located on the mean water-free surface at an appropriate location. The positive unit vector $\underline{n}_1$ points towards the North, $\underline{n}_2$ points towards the East, and $\underline{n}_3$ points downwards.
- The b-frame $\{\boldsymbol{\Omega}_I, \underline{b}_i\}$ is fixed to the vessel hull.The origin, $\boldsymbol{\Omega}_I = x_I \underline{n}_1 + y_I \underline{n}_2$, is located in the middle of the ship length taken along the symmetry axes, and on the waterline. The positive unit vector $\underline{b}_1$ points towards the bow, $\underline{b}_2$ points towards starboard, and $\underline{b}_3$ points downwards.
- The d-frame $\{\boldsymbol{\Omega}_{WP_1}, \underline{d}_i\}$ is fixed with the path defined by the two waypoints selected at each time step ($\boldsymbol{\Omega}_{WP_1}$ and $\boldsymbol{\Omega}_{WP_2}$) by the track keeping guidance. The origin is in $\boldsymbol{\Omega}_{WP_1} = x_{WP_1} \underline{n}_1 + y_{WP_1} \underline{n}_2$, the positive vector $\underline{d}_1$ points towards the vector $(\boldsymbol{\Omega}_{WP_2} - \boldsymbol{\Omega}_{WP_1})$, $\underline{d}_2$ points towards starboard, and $\underline{d}_3$ points downwards.
- The l-frame $\{\boldsymbol{\Omega}_L, \underline{l}_i\}$ is fixed with the on-board LiDAR sensor and is the system in which the point cloud is acquired. Its orientation with respect to system $\underline{b}$ frame depends on the installation and can be modelled as a heading bias δ_ψ.

 https://doi.org/10.24868/11141

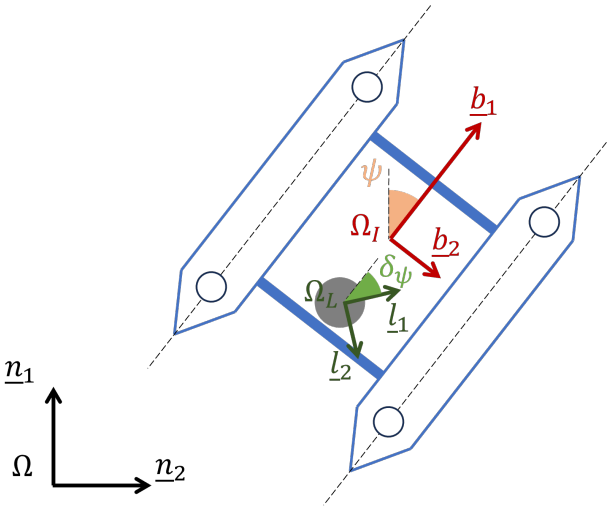

Figure 2: Reference frames.

The reference systems lie in the same plane and are related by the Euler angle and the relative rotations in (1). The generic rotation matrix is shown in (2).

$$\underline{n} = \boldsymbol{R}(\psi)\,\underline{b}, \quad \underline{n} = \boldsymbol{R}(\xi)\,\underline{d}, \quad \underline{n} = \boldsymbol{R}(\psi + \delta_\psi)\,\underline{l}, \tag{1}$$

$$\boldsymbol{R}(\star) = \begin{bmatrix} \cos\star & -\sin\star & 0 \\ \sin\star & \cos\star & 0 \\ 0 & 0 & 1 \end{bmatrix} \tag{2}$$

where ψ is the heading angle, ξ is the angle defined by the vector $(\boldsymbol{\Omega}_{WP_2} - \boldsymbol{\Omega}_{WP_1})$ and $\underline{n}_1$, δ_ψ is the installation heading bias of the LiDAR sensor, and $\star$ is the generic angle between the selected reference frames.

The adopted pose $\boldsymbol{\eta} = [x, y, \psi]$ and speed $\boldsymbol{\nu} = [u, v, r]$ arrays in this paper are, respectively, the positions with respect to the origin of the $\underline{n}$ frame and the heading angle, and the speed components in the $\underline{b}$ frame.

4 Coverage-based guidance strategy

The guidance system aims to compute proper paths and trajectories to guarantee the surveillance of a given Area Of Interest (AOI), i.e. the survey domain, with three subsystems as shown in Figure 1.

The coverage subsystem is the core of the proposed guidance strategies. It is responsible for implementing the high-level guidance, i.e. generating target locations $\mathbf{WP}_{target}$ to fulfil the surveillance mission. The target locations are generated to comply with two constraints: the randomness of the surveillance path and the coverage of the AOI.

To comply with these constraints a Markov Chain-based stochastic coverage algorithm is developed. A Markov Chain is a triple $(\mathcal{M}, \mathcal{G}, m)$ where $\mathcal{M}$ is a stochastic matrix, $\mathcal{G}$ is a connected graph representing the locations in the AOI, and m is the final state of the chain, that corresponds, in this application, to the probability of the MASS being in a specific location after an infinite number of jumps.

The developed stochastic algorithm proceeds as follows. Let $\mathcal{D}$ be a connected domain and $\mathcal{P}$ be a partition of it. The centroids of the elements of $\mathcal{P}$ are the states of the Markov Chain, i.e. the nodes of $\mathcal{G}$, and represent the target locations that the MASS will visit during the surveillance mission. At each iteration, the stochastic coverage algorithm removes from all available locations, i.e. the elements of $\mathcal{P}$, those within a distance d_{prox} from the MASS current location. The new $\mathbf{WP}_{target}$ is chosen randomly from the remaining cells according to a uniform probability distribution. This process is repeated each time the MASS reaches the previously generated target location. The distance d_{prox} is introduced to avoid that the $\mathbf{WP}_{target}$ is too close to the MASS current location. The random choice of $\mathbf{WP}_{target}$ ensures the randomness of the surveillance path, while the coverage of the AOI is ensured by the irreducibility of the Markov Chain, which is ensured by the connectedness of $\mathcal{D}$ (Duan and Bullo, 2021).

The collision-free path planning subsystem is responsible for implementing the guidance path planning and the reactive layer, i.e. it computes a collision-free path as a series of waypoints each time a new target location is computed by the coverage subsystem or each time the MASS faces the risk of collision. It takes as input the pose of the MASS $\boldsymbol{\eta}$, its speed $\boldsymbol{\nu}$, the occupancy grid of the domain, and a target location $\mathbf{WP}_{target}$. The algorithm adopted is described in (Zaccone and Martelli, 2018) and is based on a Rapidly exploring Random Tree (RRT*) path planning algorithm. Several cost functions can be adopted; in this paper, the choice is to penalise longer paths.

 https://doi.org/10.24868/11141

The first two subsystems of the guidance system can be coupled following the architecture in Figure 3. Here they act as a guidance system for a holonomic model of the MASS and this architecture can be used to test the performance of the coverage subsystem in a virtual scenario and its ability to interact with the collision-free path planning subsystem.

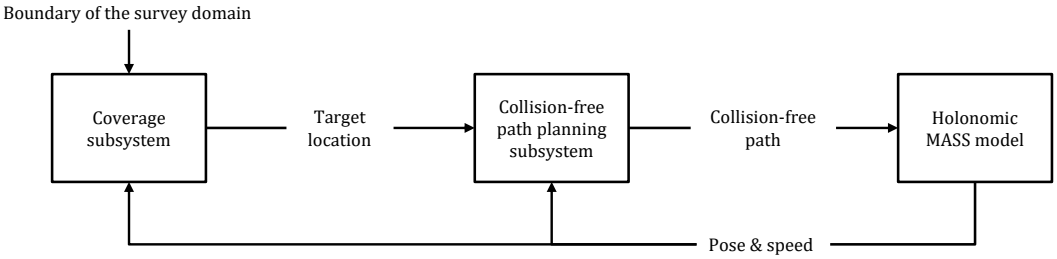

Figure 3: Coverage simulation architecture.

The track keeping subsystem follows the defined path controlling the 3-DOF of the horizontal plane as described in (Fruzzetti et al., 2024). At each time step, two consecutive waypoints are selected from $\mathbf{WP}_{list}$ and the switch at the following waypoints pair occurs when the along-track distance d_{sw} respect to $\mathbf{\Omega}_{WP_2}$ (see Figure 4a) is lower than a given distance. The speed law shown in Figure 4b is defined between each pair of waypoints. Four phases are highlighted to let an acceleration and deceleration phase between a maximum V_{max} and minimum V_{min} speed values in the proximity of the waypoints to increase the precision of the manoeuvre. The desired speed array trajectory results in (3). The desired instantaneous position $\boldsymbol{x}_d$, the yellow point in Figure 4a, is defined following the kinematics outlined by the speed law and then rotated in $\underline{n}$ to obtain $\boldsymbol{\eta}_D^*$ (4). After each switch between the pairs of waypoints, the desired angle ξ is given with a ramp establishing a heading setpoint ϕ at each time step. The resulting pose array trajectory is reported in (5).

$$\boldsymbol{\nu}_{TR} = [V(t) \;\; 0 \;\; 0]^T \tag{3}$$

$$\boldsymbol{\eta}_D^* = \boldsymbol{R}(\xi)[x_d \; 0 \; 0]^T + \mathbf{\Omega}_{WP_1} \tag{4}$$

$$\boldsymbol{\eta}_{TR} = [\boldsymbol{\eta}_D^*(1:2) \;\; \phi]^T \tag{5}$$

5 MASS state estimation feedback

Effective vessel state estimation is crucial for the guidance and control systems and to enable the MASS to fulfil its tasks effectively. Thus, the navigation system must incorporate appropriate sensing layer processing to extract valuable information and construct the state vector, measuring and estimating the necessary quantities. The vessel state estimation vessel subsystems primarily rely on a Linear Kalman Filter (LKF) (Maybeck, 1990) with a fully kinematic constant velocity state transition model. Since the LKF state-space model is expressed in the inertial $\underline{n}$ frame, the speed component of the state $\boldsymbol{x}$ are rotated in the body frame $\underline{b}$ following the rotations in (1) to lead to the feedback state $\boldsymbol{x}_{fbk} = [\boldsymbol{\eta}, \boldsymbol{\nu}]$.
Mainly, two use cases are planned: indoor preliminary tests and operational environment missions with the consequent use of a dedicated sensing layer for each setup, as shown in Figure 5. Both setups are based on the same LKF, which is adapted to receive a different measurement $\boldsymbol{z}$ by adjusting the observation matrix and the error models of the filter. Indeed, GPS cannot be used appropriately during indoor tests necessary for preliminary validations due

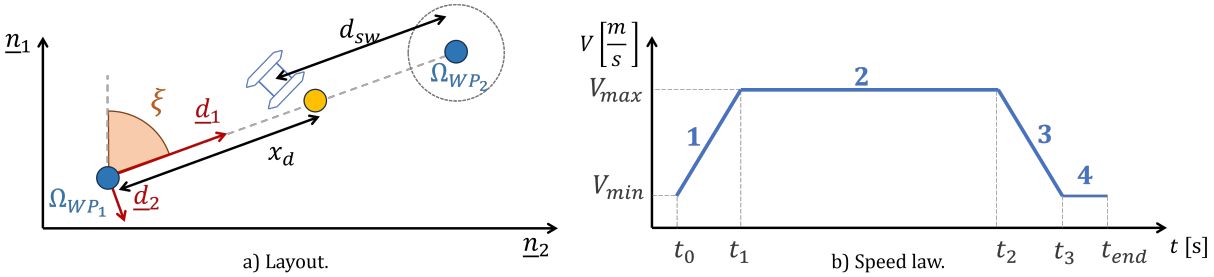

Figure 4: Track Keeping motion control scenario.

 https://doi.org/10.24868/11141

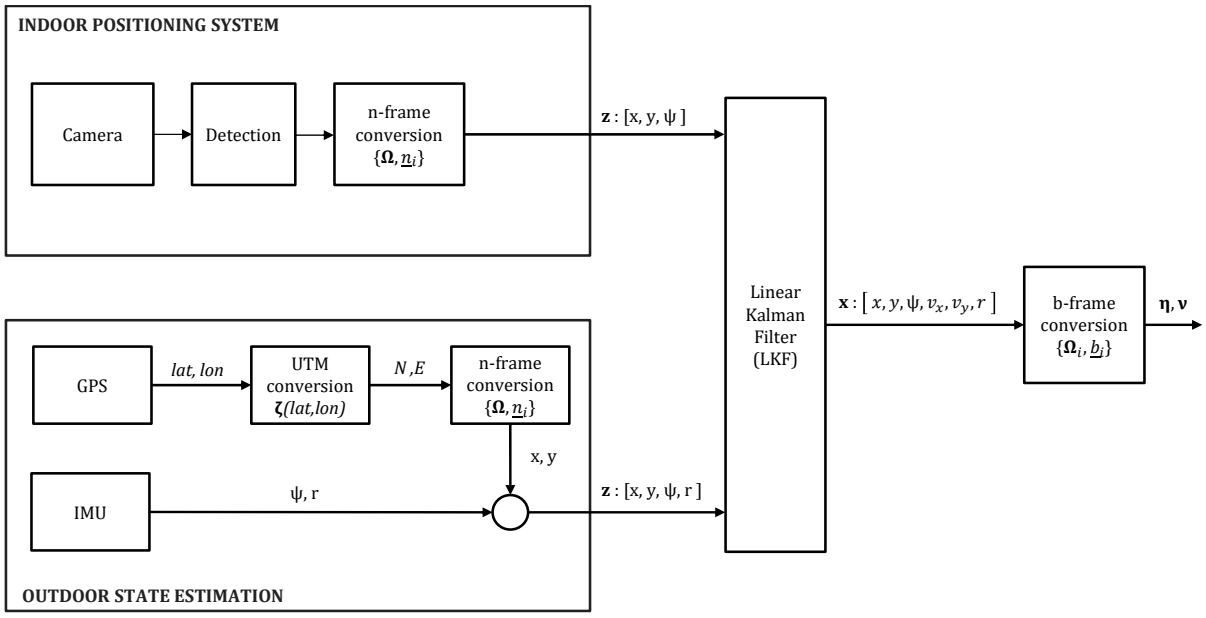

Figure 5: State estimation general pipeline.

to the lack of line-of-sight with satellites; hence, the Indoor Positioning System (IPS) presented in (Ponzini et al., 2023) is used. The resulting LKF measurement vector $\boldsymbol{z}$ is $[x, y, \psi]$, and the system can ensure the tests of development logic from the initial steps since the onboard mounted proprioceptive sensors are not involved. During the operating life, the vehicle state must be estimated based on the onboard GPS and IMU. The GPS provides the latitude and longitude measures, while the IMU provides the heading angle ψ and the rate of turn r via the embedded gyroscope and magnetometer. The general GPS position $(lat_{\boldsymbol{p}}, lon_{\boldsymbol{p}})$ is first reported in Universal Transverse Mercator (UTM) coordinates (Snyder, 1987), using local Easting and Northing coordinates. Then, considering the inertial $\underline{n}$ frame placed in the suitable location $\boldsymbol{\Omega}$ of known coordinates $(lat_{\boldsymbol{\Omega}}, lon_{\boldsymbol{\Omega}})$, GPS position data can be expressed in the $\underline{n}$ frame according to (6). The resulting LKF measurement vector $\boldsymbol{z}$ is $[x, y, \psi, r]$.

$$\boldsymbol{z}(1:2) = \boldsymbol{\zeta}(lat_{\boldsymbol{P}}, lon_{\boldsymbol{P}},) - \boldsymbol{\zeta}(lat_{\boldsymbol{\Omega}}, lon_{\boldsymbol{\Omega}}) \tag{6}$$

where $\boldsymbol{\zeta}$ refers to the UTM conversion function.

6 Environmental perception

Environmental perception aims to obtain information on the surrounding obstacles and targets and is crucial to safely and effectively fulfilling the mission goal. In this paper, environmental perception is entrusted to an onboard LiDAR and the obstacle detection is achieved using the occupancy grid method. Such an approach allows for fast and streamlined processing, bypassing time-consuming clustering methods, and can be effectively integrated with GIS data (Goodchild, 2009). The point cloud $\boldsymbol{X}^{LiDAR}$ is first projected onto the $\underline{l}_1, \underline{l}_2$ plane defined by the $\underline{l}$ frame and is sub-sampled to construct a list of obstacle-point $\boldsymbol{\Lambda}^{LiDAR}$. The domain is divided into a grid of size ϵ, and each box occupied by at least one point of the LiDAR point cloud is considered full, leading to an obstacle point placed in its centroid. A large obstacle can be rendered with only a few obstacle points choosing the ϵ parameter compatibly with the collision-free path planner detailed in Section 4. This allows the rich information set of the point cloud $\boldsymbol{X}^{LiDAR}$ to be condensed into a lean list of obstacle-points $\boldsymbol{\Lambda}^{LiDAR}$, obtaining the same result.

7 Shadow vessels monitoring

The obstacle-point set obtained from the environmental perception subsystem can be exploited to detect anomalies in the AOI, like dark ships/shadow vessels, and achieve the surveillance goal.

In this paper, the search is primarily oriented to AIS unequipped vessels or ones that intentionally keep it off and are not detectable by long-range RADARs. By cross-referencing GIS data, other prior information data such as AIS, and the obtained LiDAR point cloud, intruder vessels can be detected by subtraction. Figure 6 illustrates the entire shadow vessel detection pipeline. The MASS strategic operational environment is considered known; GIS morphology data are available, as well as other a priori information (AIS data, navigation information, etc.). The onboard LiDAR acquires the point cloud of the surrounding environment in $\underline{l}$ frame. A sub-sampled list of

 https://doi.org/10.24868/11141

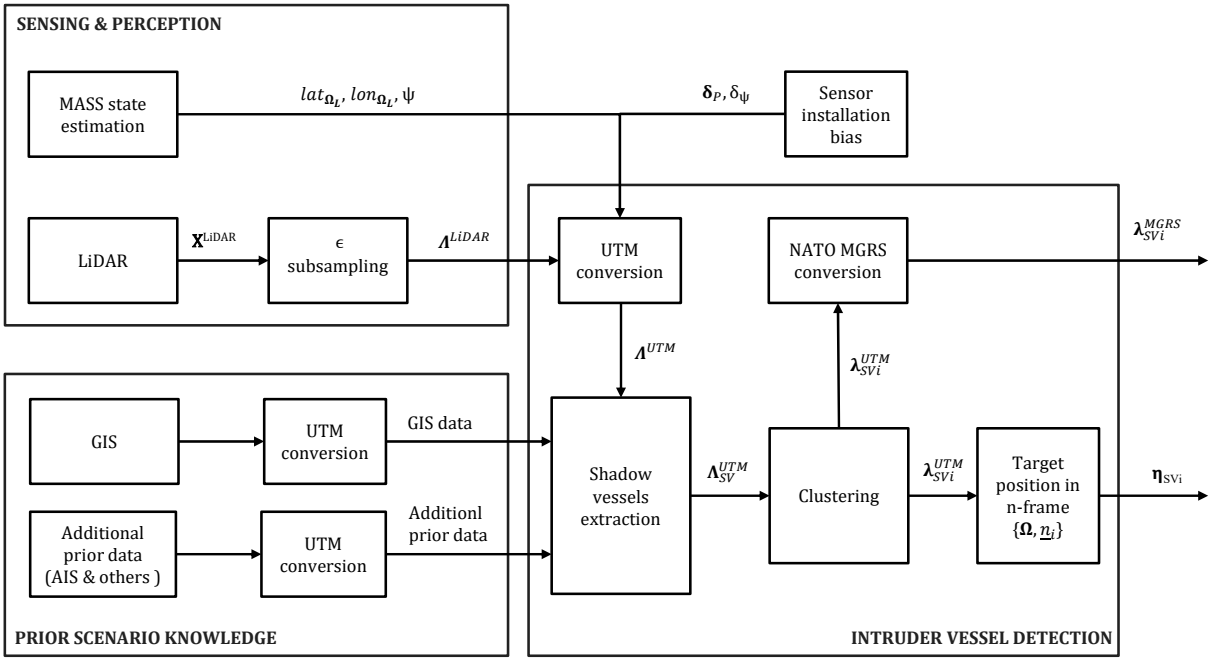

Figure 6: shadow vessels monitoring pipeline.

obstacle points $\boldsymbol{\Lambda}^{LiDAR}$ is derived from $\boldsymbol{X}^{LiDAR}$, according to Section 6, to reduce computational load. The obstacle points are then reported in UTM Easting-Northing coordinates ($\boldsymbol{\Lambda}^{UTM}$) according to (7), knowing the pose η of the supervising MASS by the state estimation feedback as given in Section 5. A likely bias $\boldsymbol{\delta}_P = \epsilon_x \underline{l}_1 + \epsilon_y \underline{l}_2$ on the position of LiDAR and GPS receiver is considered due to physical installation, in addition to the LiDAR installation bias δ_ψ.

$$\boldsymbol{\Lambda}^{UTM} = \boldsymbol{R}(\psi + \delta_\psi)\boldsymbol{\Lambda}^{LiDAR} + \boldsymbol{R}(\psi + \delta_\psi)\boldsymbol{\delta}_P + \boldsymbol{\zeta}(lat_{\boldsymbol{\Omega_L}}, lon_{\boldsymbol{\Omega_L}}) \tag{7}$$

All multi-source information is expressed in the same UTM reference frame, extracting on a geometrical basis the obstacle points that do not belong to any expected agent, i.e. spotting the shadow vessels. A buffer zone around known objects is carefully selected to mitigate sensor, positioning, and ego-motion errors. The $\boldsymbol{\Lambda}^{UTM}$ obstacle-points list is thus divided into environment-related obstacles $\boldsymbol{\Lambda}_{env}^{UTM}$, including information about objects known in advance, and shadow-vessel obstacle-points $\boldsymbol{\Lambda}_{SV}^{UTM}$.

Unsupervised learning clustering is used to separate individual shadow-vessels within the obstacle-points list $\boldsymbol{\Lambda}_{SV}^{UTM}$ providing a set of single vessel obstacle-points cluster $\boldsymbol{\lambda}_{SVi}^{UTM}$; by iterating through the list of clusters, the location of each can be easily calculated as the average (μ) of each cluster point cloud. The UTM locations can be easily converted to NATO Military Grid Reference System (MGRS) (Hager et al., 1992), as well as expressed in the $\underline{n}$ frame, constituting part of the shadow vessel pose vector $\boldsymbol{\eta}_{SV}$, according to (8).

$$\boldsymbol{\eta}_{SV_i}(1:2) = \mu(\boldsymbol{\lambda}_{SV_i}^{UTM}) - \boldsymbol{\zeta}(lat_{\boldsymbol{\Omega}}, lon_{\boldsymbol{\Omega}}) \quad for \quad \boldsymbol{\lambda}_{SV_i}^{UTM} \quad in \quad \boldsymbol{\Lambda}_{SV}^{UTM} \tag{8}$$

8 Results

This section reports the preliminary results obtained to validate the proper functioning of the architecture and the integrability of its components. The steps to reach the final aim of testing the proposed architecture in a real critical scenario are summarised in the following phases:

I. Architecture definition and requirements specification of each subsystem needed for the integration in the overall architecture. It is done in the previous sections of this paper.

II. Individual subsystem testing (computer simulation). Each subsystem is tested individually using computer simulation. This preliminary phase is essential for subsystem development.

III. Integration and testing in a virtual scenario. Tests in a virtual scenario representing a critical infrastructure using computer simulation are carried out. The results reported for this stage include the coverage-based guidance strategy, environmental perception, and shadow vessels monitoring systems in a wind farm scenario.

 https://doi.org/10.24868/11141

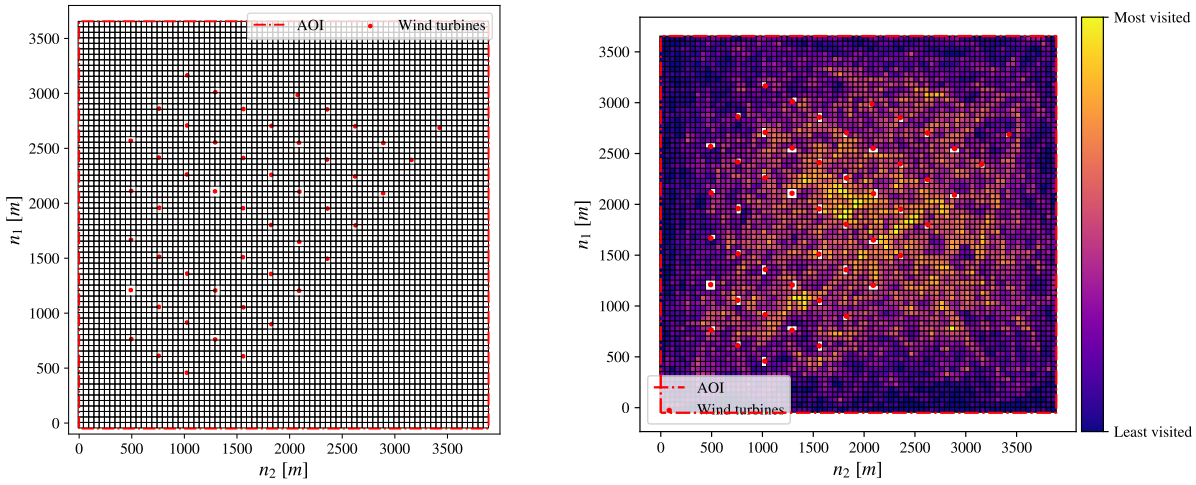

(a) Discretized AOI.

(b) Coverage algorithm final state estimate after 500 iterations.

Figure 7: Surveillance simulation.

IV. Physical MASS testing in a controlled indoor scenario. The physical MASS (SWAMP vessel) available in the university infrastructure is selected as a test bed, and selected subsystem integrations in a controlled, indoor scenario are done to verify the potential use of SWAMP. Results for this stage are reported, regarding the control system and state estimation subsystem applied to SWAMP in the university test tank.

V. Outdoor test. The selected integrated systems are used in an outdoor environment to assess functionality that is not testable in the indoor test tank; results for this stage are reported and consist of state estimation subsystem results.

VI. Complete integration and model-scale testing. The proposed architecture with the physical MASS SWAMP can be fully integrated and tested in a real environment, representing a scaled model of the critical infrastructure. It will be the object of future studies.

VII. Operative environment test. The proposed architecture can be extended to a real surveying MASS in the operative AOI. It will be the object of future studies.

The first set of results is carried out in a virtual environment representing the Lillgrund Wind Farm (Sweden) through its GIS data gathered from the Global Offshore Wind Turbine dataset (Zhang et al., 2021a). It aims to test the coverage of the selected area from the coverage algorithm, the computation of a safe path from the collision-free path planner, the capacity of the environmental perception subsystem to perceive the surrounding environment, and the identification of a possible intruder from the shadow vessels monitoring system covering testing phase III. The virtual AOI is shown in Figure 7a. The discretisation has been performed using Shapely Python library (Gillies et al., 2024) producing square-like cells of $50\,m$ sides; cells overlapping with turbines have been removed. Then, the simulation layout described in Figure 3 is applied to assess the final state m of the stochastic coverage algorithm. The resulting heatmap representing m, however, how much a cell of the discretized AOI has been visited by the holonomic model, is shown in Figure 7b. The virtual scenario is then coupled with real acquired LiDAR scans to simulate a surveillance operation where the onboard LiDAR acquires the surrounding environment, the shadow vessels monitoring system compares the ϵ sub-sampled point cloud ($\epsilon = 1\,m$) with the available GIS data, and the vessel is moving in a subset of the path previous computed and shown in magenta in Figure 8 as a polyline between the $\boldsymbol{WP_{target}}$ marked with the orange triangles, and the $\boldsymbol{WP_{list}}$ marked with the blue circles. The shadow vessels monitoring system continues to compare the LiDAR sub-sampled scans with GIS data until the presence of an intruder vessel is reported. Figure 9a shows the point cloud acquired in the virtual scenario, while Figure 9b shows the shadow vessels monitoring comparison operation. The wind turbine obstacle points are shown in blue and are superimposed on the GIS shape (brown) with its $5\,m$ buffer zone shown in green; the detected shadow vessel, not overlaying any operational environment GIS data, is marked

 https://doi.org/10.24868/11141

in red and represents $\mathbf{\Lambda}_{SV}$. From the results, it is possible to see that the objectives set have been achieved.

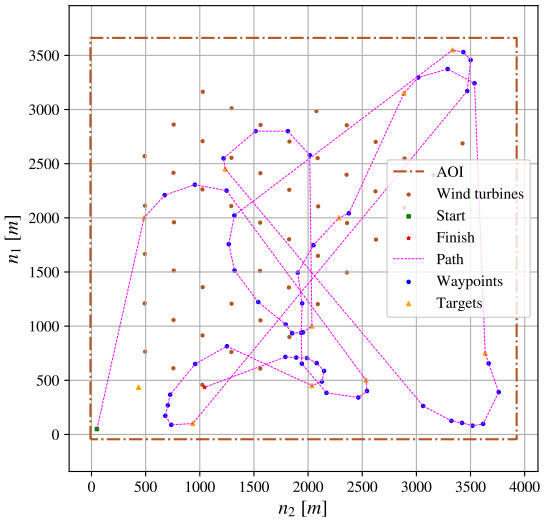

Figure 8: Slice of the surveillance path.

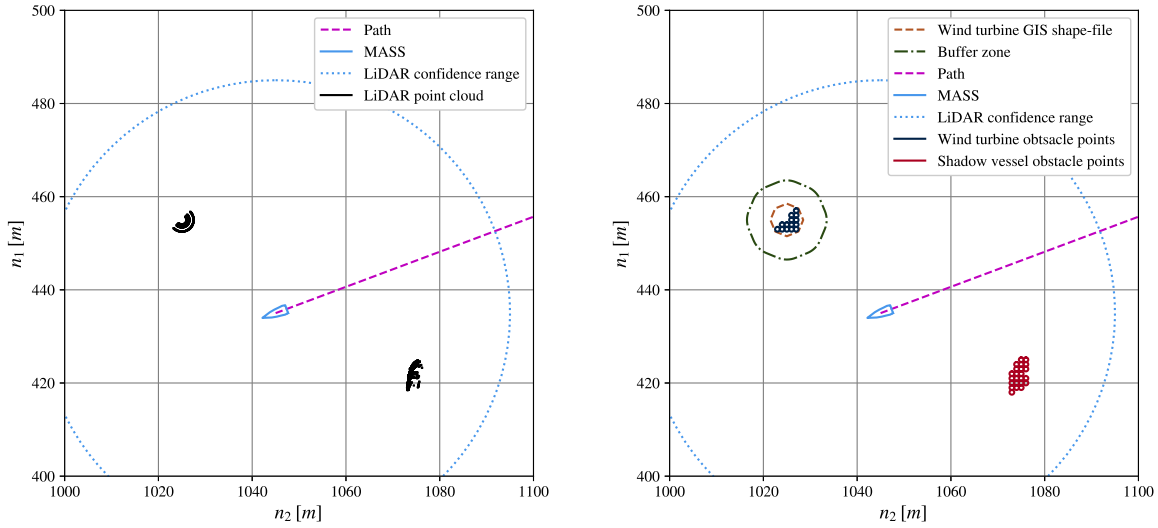

(a) LiDAR scan.

(b) Multi-source scenario.

Figure 9: shadow vessels monitoring.

The second set of results is carried out in the indoor test tank to assess the estimation and the control capability of the MASS state estimation, the control, and the track keeping subsystems, corresponding to testing phase IV. The vessel moves between four waypoints with different heading angles. The trajectory acquired from the IPS and filtered through the LKF is marked in blue in Figure 10a, where the green waterline represents the starting point and the red one identifies the endpoint. The black intermediate waterlines are aligned with the estimated heading angle and are reported at a constant time interval in real dimensions. Figure 10b shows the two speed components in $\underline{n}$ at which MASS navigated during the manoeuvre. The speeds observed through the LKF are marked in red, while the speeds calculated as a time differential from the positions are marked in black; to compare the two results, the calculated speeds are filtered via a second-order Exponential Moving Average Filter (EMAF) with a weight factor of 0.6. The results show that SWAMP can be used as a test bed and that the state estimation subsystem can be used and transported to an outdoor environment.

The third set of results covers test phase V and is carried out in an artificial lake to validate the state estimation architecture using onboard sensors. The position is acquired using GPS, while the heading angle ψ and the rotation speed r are measured with the IMU. Figure 11 presents the results obtained using the same layout adopted for pre-

 https://doi.org/10.24868/11141

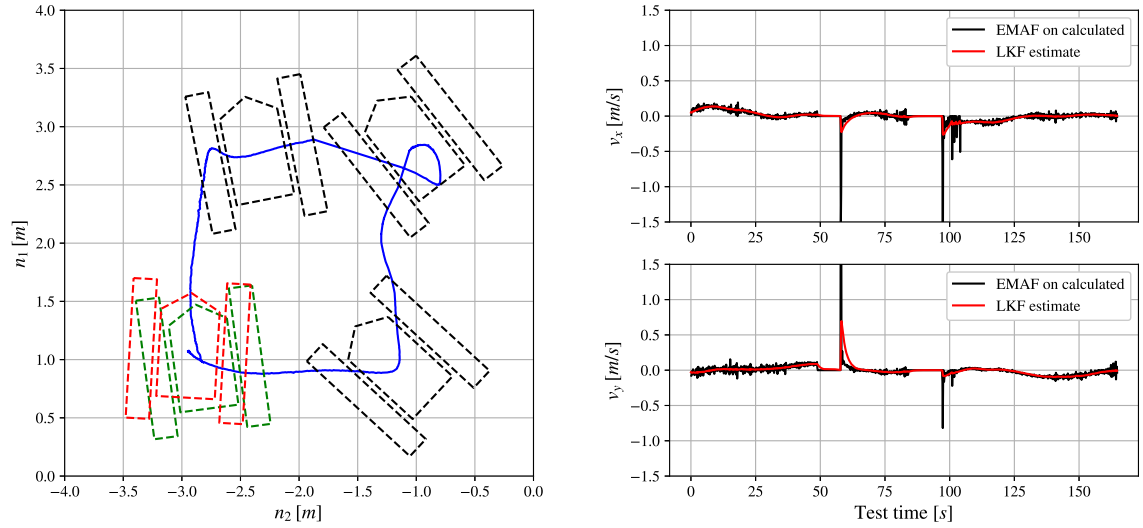

(a) Trajectory.

(b) Observed and calculated speeds.

Figure 10: Indoor experimental test.

senting the results of Figure 10. The higher spikes observed are attributed to the greater measurement error of the GPS if compared to the indoor IPS and to the different acquisition frequencies. Despite the noisy measurement, the filter effectively estimates the velocities, mitigating sudden oscillations. The results show that the state estimation system can also be used successfully outdoors.

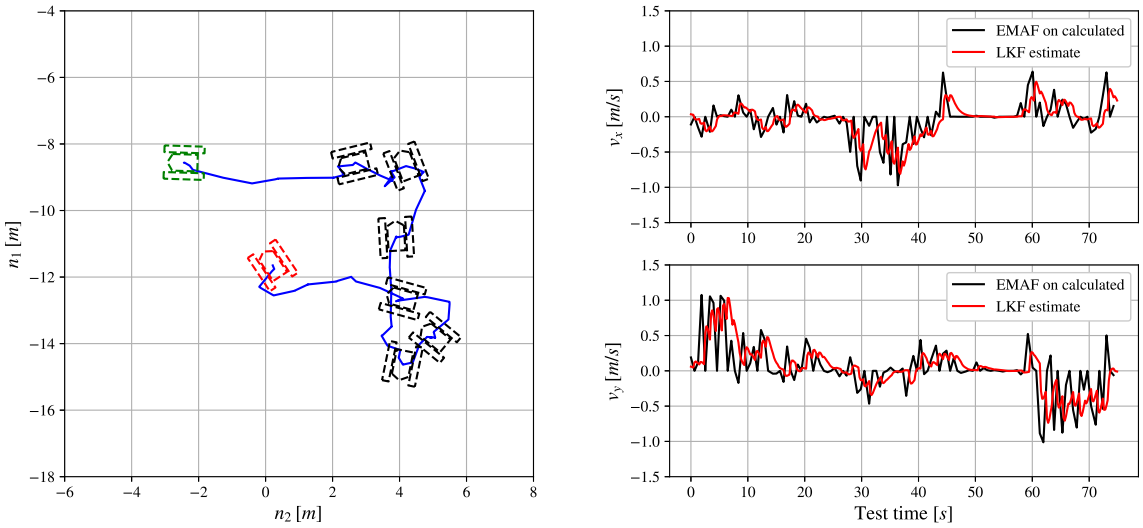

(a) Trajectory.

(b) Observed and calculated speeds.

Figure 11: Outdoor experimental test.

9 Conclusions and further research

This paper presents a MASS architecture for critical infrastructure monitoring missions. The preliminary results obtained and presented demonstrate the ability of the proposed architecture to achieve its proper functioning and the integrability of its components. The real data-based simulation of the high-level guidance and perception coupled systems shows the ability of the proposed architecture to safely and effectively patrol an area of strategic

 https://doi.org/10.24868/11141

importance, detecting anomalies by cross-referencing LiDAR acquisitions with multi-source information. The tests in indoor and outdoor controlled environments demonstrate the architecture ability to control the MASS and estimate its state as well as the integrability of the proposed systems, capable of working synergically in real-time. The limitations currently encountered concern the triggering of the reactive guidance system and environmental perception based on a single sensor and integration of the entire architecture with the consequent test in the scaled and real test case. The perceptive layer needs further improvement by incorporating multi-sensor data fusion, considering both underwater and above-the-water situational awareness. Additional studies and tests can also be carried out by integrating different frameworks to take into account the mission change when the shadow vessel is detected. Hence, a bumpless function can be added to switch to control logic in 2-DOF and apply a law that allows, for example, to follow the shadow vessel or to track the shadow vessel with reactive logic.

Acknowledgement

This research was partially funded by European Union – NextGenerationEU. Piano Nazionale di Ripresa e Resilienza, Missione 4 Componente 2 Investimento 1.4 “Potenziamento strutture di ricerca e creazione di ”campioni nazionali di R&S” su alcune Key Enabling Technologies”. Code CN00000023 – Title: “Sustainable Mobility Center (Centro Nazionale per la Mobilità Sostenibile – CNMS)”. However, views and opinions expressed are those of the author(s) only and do not necessarily reflect those of the European Union or European Commission. Neither the European Union nor the granting authority can be held responsible.

References

Birk, A., Pascoal, A., Antonelli, G., Caiti, A., Casalino, G., Indiveri, G., Caffaz, A., 2012. Cooperative Cognitive Control for Autonomous Underwater Vehicles (CO3AUVs): overview and progresses in the 3rd project year. IFAC Proceedings Volumes 45, 361–366. doi:https://doi.org/10.3182/20120410-3-PT-4028.00060. 3rd IFAC Workshop on Navigation, Guidance and Control of Underwater Vehicles.

Bueger, C., 2023. Russian Spy Ship in North Sea raises concerns about the vulnerability of key maritime infrastructures. URL: https://theconversation.com/russian-spy-ship-in-north-sea-raises-concerns-about-the-vulnerability-of-key-maritime-infrastructure-204205. accessed on 13/05/2024.

Bueger, C., Liebetrau, T., 2023. Critical maritime infrastructure protection: What’s the trouble? Marine Policy 155, 105772. doi:https://doi.org/10.1016/j.marpol.2023.105772.

Chataut, R., 2024. Undersea cables are the unseen backbone of the global internet. URL: https://theconversation.com/undersea-cables-are-the-unseen-backbone-of-the-global-internet-226300.

Clare, M., 2021. Submarine Clable Protection and the Environment. An Update from the ICPC. URL: https://www.iscpc.org/publications/submarine-cable-protection-and-the-environment/ICPC_Public_EU_March%202021.pdf.

Commission, E., 2023. Eu Wind Power Action Plan. URL: https://eur-lex.europa.eu/legal-content/EN/TXT/PDF/?uri=CELEX:52023DC0669.

Donnarumma, S., Fruzzetti, C., Martelli, M., Chiti, R., Pecoraro, A., Sebastiani, L., 2022. Rapid prototyping for enhanced dynamic positioning systems, p. 641 – 649. doi:10.3233/PMST220075.

Duan, X., Bullo, F., 2021. Markov chain–based stochastic strategies for robotic surveillance. Annual Review of Control, Robotics, and Autonomous Systems 4, 243–264. doi:https://doi.org/10.1146/annurev-control-071520-120123.

Faggioni, N., Leonardi, N., Ponzini, F., Sebastiani, L., Martelli, M., 2022a. Obstacle Detection in Real and Synthetic Harbour Scenarios, in: Modelling and Simulation for Autonomous Systems, Springer International Publishing, Cham. pp. 26–38. doi:https://doi.org/10.1007/978-3-030-98260-7_2.

Faggioni, N., Ponzini, F., Martelli, M., 2022b. Multi-obstacle detection and tracking algorithms for the marine environment based on unsupervised learning. Ocean Engineering 266, 113034. doi:https://doi.org/10.1016/j.oceaneng.2022.113034.

Ferri, G., Munafò, A., Tesei, A., Braca, P., Meyer, F., Pelekanakis, K., Petroccia, R., Alves, J., Strode, C., LePage, K., 2017. Cooperative robotic networks for underwater surveillance: an overview. IET Radar, Sonar & Navigation 11, 1740–1761. doi:https://doi.org/10.1049/iet-rsn.2017.0074.

Fossen, T.I., 2011. Handbook of marine craft hydrodynamics and motion control. John Wiley & Sons. doi:10.1002/9781119994138.

Fruzzetti, C., Donnarumma, S., Martelli, M., Maggiani, F., 2022. Dynamic positioning operability assessment by using thrust allocation optimization, in: Sustainable Development and Innovations in Marine Technologies. CRC Press, pp. 25–32.

Fruzzetti, C., Martelli, M., Lekkas, A., Skjetne, R., Breivik, M., 2024. Model-based motion control design for the

milliampere1 prototype ferry, in: 2024 European Control Conference (ECC), pp. 3636–3643. doi:10.23919/ECC64448.2024.10591071.

Gillies, S., van der Wel, C., Van den Bossche, J., Taves, M.W., Arnott, J., Ward, B.C., et al., 2024. Shapely. URL: https://github.com/shapely/shapely, doi:10.5281/zenodo.5597138.

Goodchild, M.F., 2009. Geographic information systems and science: today and tomorrow. Procedia Earth and Planetary Science 1, 1037–1043. doi:https://doi.org/10.1016/j.proeps.2009.09.160. special issue title: Proceedings of the International Conference on Mining Science & Technology (ICMST2009).

Hager, J.W., Fry, L.L., Jacks, S.S., Hill, D.R., 1992. Datums, Ellipsoids, Grids, and Grid Reference Systems. Defense Technical Information Center. doi:10.21236/ada247651.

Jolly, Claire, O., 2016. The ocean economy in 2030, in: Proceedings of the Workshop on Maritime Cluster and Global Challenges 50th Anniversary of the WP6, Paris, France. doi:https://doi.org/10.1787/9789264251724-en.

Jouffray, J.B., Blasiak, R., Norström, A.V., Österblom, H., Nyström, M., 2020. The Blue Acceleration: The Trajectory of Human Expansion into the Ocean. One Earth 2, 43–54. doi:https://doi.org/10.1016/j.oneear.2019.12.016.

Kantchev, G., 2023. Sweden Says Second Undersea Cable Damaged in Baltic Sea. URL: https://www.wsj.com/world/europe/sweden-says-second-undersea-cable-damaged-in-baltic-sea-d9f21fea.

Karaki, A.A., Bibuli, M., Caccia, M., Ferrando, I., Gagliolo, S., Odetti, A., Sguerso, D., 2022. Multi-Platforms and Multi-Sensors Integrated Survey for the Submerged and Emerged Areas. Journal of Marine Science and Engineering 10. doi:10.3390/jmse10060753.

Knights, M., 2024. Assessing the Houthi War Effort Since October 2023. URL: https://www.washingtoninstitute.org/policy-analysis/assessing-houthi-war-effort-october-2023.

Manzari, D.T.L.B.A.C.R.C.V., 2020. Marine Robots for Underwater Surveillance doi:https://doi.org/10.1007/s43154-020-00028-z.

Martelli, M., Faggioni, N., Ponzini, F., 2022. Detecting and Tracking Multi-Object in Real Marine Environment, in: Proceedings of the International Ship Control Systems Symposium. doi:https://doi.org/10.24868/10707.

Maybeck, P.S., 1990. The Kalman Filter: An Introduction to Concepts. Springer New York, New York, NY. pp. 194–204. doi:10.1007/978-1-4613-8997-2_15.

Molina-Molina, J.C., Salhaoui, M., Guerrero-González, A., Arioua, M., 2021. Autonomous marine robot based on ai recognition for permanent surveillance in marine protected areas. Sensors 21, 2664. doi:https://doi.org/10.3390/s21082664.

Nguyen, T., 2023. The challenges of dark ships to the safety and security of commercial shipping and the way forward. Asia-Pacific Journal of Ocean Law and Policy 8, 310 – 328. URL: https://brill.com/view/journals/apoc/8/2/article-p310_007.xml.

Odetti, A., Bruzzone, G., Altosole, M., Viviani, M., Caccia, M., 2020. SWAMP, an autonomous surface vehicle expressly designed for extremely shallow waters. Ocean Engineering 216, 108205. doi:https://doi.org/10.1016/j.oceaneng.2020.108205.

Ponzini, F., Zaccone, R., Martelli, M., 2023. A multi-sensor indoor tracking system for autonomous marine model-scale vehicles. Journal of Physics: Conference Series 2618, 012008. doi:10.1088/1742-6596/2618/1/012008.

Snyder, J.P., 1987. Map projections: A working manual, in: Professional Paper. U.S. Government Printing Office. volume 1395. doi:https://doi.org/10.3133/pp1395.

Song, R., Liu, Y., Bucknall, R., 2019. Smoothed A* algorithm for practical unmanned surface vehicle path planning. Applied Ocean Research 83, 9–20. doi:https://doi.org/10.1016/j.apor.2018.12.001.

Tan, C.S., Mohd-Mokhtar, R., Arshad, M.R., 2021. A Comprehensive Review of Coverage Path Planning in Robotics Using Classical and Heuristic Algorithms. IEEE Access 9, 119310–119342. doi:10.1109/ACCESS.2021.3108177.

UNCTAD, 2017. Review of Maritime Transport 2017. URL: https://unctad.org/system/files/official-document/rmt2017_en.pdf.

UNCTAD, 2022. Review of Maritime Transport 2022. URL: https://unctad.org/system/files/official-document/rmt2022_en.pdf.

Yassein, M.B., Shatnawi, M.Q., Aljwarneh, S., Al-Hatmi, R., 2017. Internet of Things: Survey and open issues of MQTT protocol, in: 2017 International Conference on Engineering & MIS (ICEMIS), pp. 1–6. doi:10.1109/ICEMIS.2017.8273112.

Zaccone, R., 2024. A dynamic programming approach to the collision avoidance of autonomous ships. Mathematics 12. doi:10.3390/math12101546.

Zaccone, R., Martelli, M., 2018. A random sampling based algorithm for ship path planning with obstacles, in: Conference Proceedings of iSCSS. doi:https://doi.org/10.24868/issn.2631-8741.2018.018.

Zadeh, S.M., Abbasi, A., Yazdani, A., Wang, H., Liu, Y., 2022. Uninterrupted path planning system for Multi-USV sampling mission in a cluttered ocean environment. Ocean Engineering 254, 111328. doi:https://doi.org/10.1016/j.oceaneng.2022.111328.

Zhang, T., Tian, B., Sengupta, D., Zhang, L., Si, Y., 2021a. Global offshore wind turbine dataset. Scientific Data 8, 191.

Zhang, W., Jiang, F., Yang, C.F., Wang, Z.P., Zhao, T.J., 2021b. Research on Unmanned Surface Vehicles Environment Perception Based on the Fusion of Vision and Lidar. IEEE Access 9, 63107–63121. doi:10.1109/ACCESS.2021.3057863.